M. Short
School of Mechanical Engineering,
Purdue University,
West Lafayette, IN 47907
e-mail: short44@purdue.edu

T. Siegmund
School of Mechanical Engineering,
Purdue University,
West Lafayette, IN 47907
e-mail: siegmund@purdue.edu

Scaling, Growth, and Size Effects on the Mechanical Behavior of a Topologically Interlocking Material Based on Tetrahedra Elements

The present study is concerned with the deformation response of an architectured material system, i.e., a 2D-material system created by the topological interlocking assembly of polyhedra. Following the analogy of granular crystals, the internal load transfer is considered along well-defined force networks, and internal equivalent truss structures are used to describe the deformation response. Closed-form relationships for stiffness, strength, and toughness of the topologically interlocked material system are presented. The model is validated relative to direct numerical simulation results. The topologically interlocked material system characteristics are compared with those of monolithic plates. The architectured material system outperforms equivalent size monolithic plates in terms of toughness for nearly all possible ratios of modulus to the strength of the material used to make the building blocks and plate, respectively. In addition, topologically interlocked material systems are shown to provide better strength characteristics than a monolithic system for low strength solids. [DOI: 10.1115/1.4044025]

1 Introduction

Plates are planar structural elements that can carry transverse mechanical loads. Theories for the analysis of deflection and stresses in plates as continuous solids have been established [1], including those for thin and thick plates. It is however not necessary that a transverse load carrying structure should be monolithic. In several studies [2–5], it has been demonstrated that arranging polyhedra in topological interlocking geometric configurations also leads to a planar system that can carry transverse load. In the same way as graphene is considered a 2D material (sometimes described by a continuum plate theory), the assembly of polyhedra is also considered as a 2D material, i.e., a topologically interlocked material (TIM) system. Since in TIM systems, the mechanical response emerges from geometry (the polyhedra geometry and assembly) with the building blocks larger than the microscopic features of the material used to make the building block, TIM systems are included in the emerging class of architectured material systems [4]. In TIM systems, the overall deformation response of the planar assembly subjected to a transverse load emerges from the elastic deformation of the unit building blocks and from contact and sliding between building blocks. For these material systems, several interesting mechanical properties have been demonstrated, and past studies have applied several different analysis approaches to interpret the experimental findings.

Computational models using discrete element methods [6] or finite element computations [7] directly mirror the experimental observations on the mechanical response of TIM systems but lack generality in their outcomes. Analytical methods consider a partially cracked beam analogy [8], a masonry approach [9], a thrust line approach motivated by a granular material analogy [7,10], an augmented continuum mechanics homogenization approach [11], or on a model combining block sliding and elastic deformation [12].

Here, the thrust line approach is followed. This considers TIM systems as granular crystals, i.e., an arrangement of macroscopic particles on a lattice, and relates the internal load transfer in the TIM system to the arrangement of the building blocks. Then, the internal structure of the force network can be defined. An equivalent truss structure representing the material in the volume occupied by the force network can be established, and the deformation of the equivalent truss structure is used to identify the mechanical response of the TIM system. The present work thereby extends prior work by the authors on the elastic TIM response to predictions of strength and toughness.

The analysis presented here is performed for one key topological interlocking configuration, which is the densest planar packing of tetrahedra. Square-shaped assemblies are supplemented with boundary conditions and subjected to a central load. Finally, a comparison to equivalent monolithic plates is performed.

2 Experiment

Topologically interlocked material systems are assemblies of all identical and convex polyhedra. The specific system of consideration in this study is based on tetrahedra building blocks of edge length a_0 (Fig. 1(*a*)), arranged in a planar configuration. Two pairs of tetrahedra (AA and BB) constrain a central tetrahedra (C) against the motion in two axes. The resulting 2D assembly corresponds to the densest planar packing of tetrahedra [13]. Figure 1(*b*) depicts a drawing of an assembly with $N^2 = 49$ tetrahedra.

An external constraint structure is required (Fig. 1(*b*)) which is provided by four wedge-shaped bodies. The boundary provides the in-plane constraint confining the granular system. The boundary also acts as a support for the transverse loading configuration. With the wedge shape boundary bodies, the tetrahedra to boundary element contact is only half of that when compared with the tetrahedra to tetrahedra contacts in the interior of the assembly. Consequently, tetrahedra at the boundary are only partially constraint, allowing for their rotation relative to the assembly plane.

The internal load transfer following from transverse loading is visualized by the use of a photoelastic experiment. A TIM system

Contributed by the Applied Mechanics Division of ASME for publication in the Journal of Applied Mechanics. Manuscript received April 15, 2019; final manuscript received June 3, 2019; published online June 17, 2019. Assoc. Editor: Francois Barthelat.

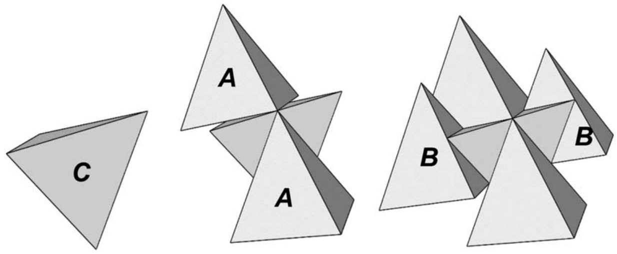

(*a*)

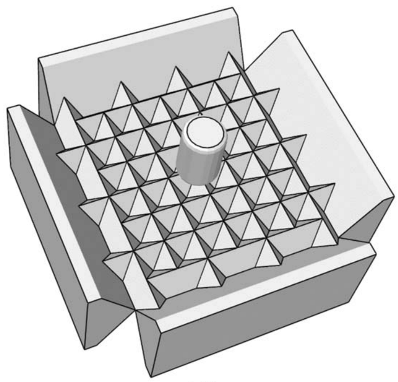
(*b*)

Fig. 1 Interlocking assembly of tetrahedra of edge length a_0: (*a*) assembly process and (*b*) assembly with $N^2=49$ tetrahedra with supports and transverse point loading

with $N^2=49$ tetrahedra of the edge length of $a_0=25$ mm was considered. The number of tetrahedra along one edge of the square assembly (Fig. 1(*b*)) is N. The TIM system was additively manufactured using of a Connex 350 Polyjet printer with the manufacturer supplied VeroClear resin and FullCure 705 Support resin (Stratasys™). All 49 building blocks and the surrounding support were printed as a combined assembly with the support resin printed to fill any overhang and all gaps between building blocks. A gap of 0.2 mm between parts of the assembly is used to enable the release of each of the parts from its neighbors. The tetrahedra-to-tetrahedra gap is filled with support material during printing. The as-printed TIM system was cleaned by use of a waterjet to remove the support material, including that filling the gaps between adjacent parts. Shim stock was inserted between the surrounding support structure and the tetrahedra.

Photoelastic experiments have been used to determine the load transfer pattern in 2D granular solids under in-plane confinement and loads [14]. Parts made of the Veroclear resin are photoelastic. For the photoelasticity-based investigation of the load transfer pattern in TIM systems, the experimental setup needs to be designed to allow for the photoelastic visualization under consideration of out-of-plane stress components. The photoelastic visualization setup consists of a light table covered with a linear polarizing film sheet. The transparent 3D-printed TIM system was placed on top of the light table using a rigid support structure to provide a free space between the light table and the TIM system. A C-clamp was used to impose a deflection onto the center of the TIM system, and the light table provided the opposing reaction. A monochrome CCD camera equipped with a polarizing lens was placed with the optical axis aligned normal to the TIM system plane (i.e., parallel to the action of the loading device) used to record the photoelastic darkfield image. The photoelastic experiment provides a darkfield image where regions of high stresses are brighter.

Figure 2(*a*) depicts the image from the transverse loading of the TIM system built from photoelastic building blocks. The experiment reveals that the load transfer in the TIM system is distinctly different from that in a monolithic plate under equivalent loading and boundary conditions. The internal load transfer can be characterized by the formation of force networks leading to discrete locations where reaction forces occur (Fig. 2(*b*)).

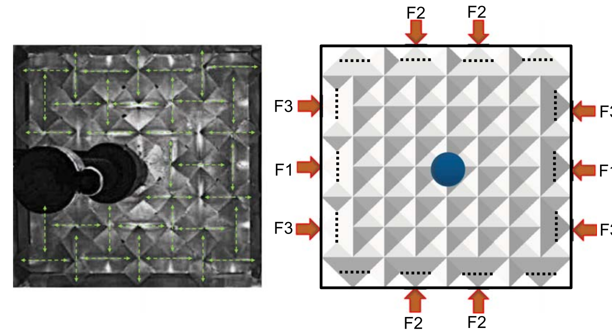

(*a*) (*b*)

Fig. 2 (*a*) Photoelastic image of a transversely loaded topologically interlocked material system ($a_0=25$ mm, $N^2=49$). In the darkfield image, bright regions correspond to higher stresses. Green lines indicate the location and orientation of the tetrahedra edges on the top surface of the assembly. (*b*) Corresponding sketch of the topologically interlocked material system. Vectors indicate locations of load transfer to the support corresponding to force network paths F1, F2, and F3. The center circle is the location of the load application. Dashed lines indicate locations where the simple support condition leads to load transfer into the support structure.

In common granular media, the under-constraint of the particle arrangement makes the force network structure non-unique. In the TIM system, all particle locations are known, and a force network structure can be proposed. In particular, for the tetrahedra assembly under a centrally applied load and the simply supported boundary conditions, a central force network paths develops starting from the point of applied load on the upper surface of the assembly, passing through the row of tetrahedra F1, and finally to the support structure where the contact between the outermost tetrahedra of F1 contacts the support on the lower surface of the assembly (Fig. 2(*b*)). Additional force network paths develop orthogonal (F2) and parallel (F3) to the central network path (F1). In noncentral network paths, no external load is applied but the topological constraints of the assembly impose a displacement field on the upper surface of the assembly such that the imposed center displacements along F2 and F3 network paths are proportional to the distance of the force network path from the externally applied load.

3 Theory

In order to construct a model for the transverse force-deflection response of the TIM system, it is necessary to consider the deformation of material elements along the force network paths. A schematic section cut along F1 in the deformed state in which the force network path in F1 is depicted (Fig. 3). In an abstraction of this configuration, it is proposed to describe the deformation of the TIM system in F1 by inscribing an equivalent Mises truss (ABCD). This approach was also confirmed by direct numerical simulation in Ref. [7]. The response of the Mises truss can be defined in terms of the geometric parameters of the unit blocks

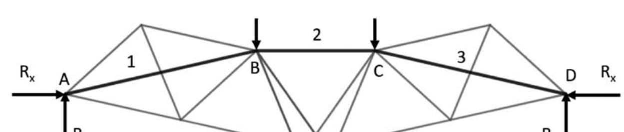

Fig. 3 Schematic of the section through the force network path F1 in the deformed configuration. An equivalent Mises truss ABCD along the force network path is used as an equivalent system to calculate the force-deflection response of the TIM system

(the tetrahedra edge length a_0 and the elastic modulus of the material used to construct the building blocks E) and the assembly (the number of tetrahedra N along the assembly edge, with the present theory restricted to square assemblies with N being an odd number). The Mises truss is supported at points A and D, where all displacements are constrained but rotations are not. Since individual building blocks interact by contact only, the Mises truss disintegrates once the angle of inclination of the forces network path with the assembly plane becomes negative, and the tensile part of the problem is irrelevant. Similar arguments are then made for the noncentral force network paths.

The span of the truss (AD) is equal to L_T and remains constant

$$L_T = a_0\left(\frac{N+1}{2}\right) = \text{const} \tag{1}$$

The height of the truss in the initial configuration is $H_0 = a_0/\sqrt{2}$. Each truss consists of three members, two lateral members (AB, CD), and one central member (BC).

In the undeformed state, the central member is parallel to the assembly plane and possesses an initial length of a_0. Furthermore, the two lateral members (AB, CD) possess an initial length of L_0 and are inclined by the angle θ_0 to the assembly plane:

$$L_0 = a_0\sqrt{\frac{1}{2}+\frac{(N-1)^2}{16}} = a_0\alpha \tag{2a}$$

$$\tan\theta_0 = \frac{H_0}{L_0} = \frac{\sqrt{2}}{2\alpha} \tag{2b}$$

The horizontal extension of the lateral members (AB, CD) in the initial configuration is $L_{0x} = a_0(N-1)/4$.

In the deformed state, the height of the truss is h, which is a function of the applied displacement v: $h = H_0 - v$. Both the two lateral members and the central member deform elastically as a displacement v is applied. The absolute values of length change of the lateral and central members (e_L and e_C, respectively) were followed from the Hooke's law.

$$e_L = \frac{F_L L_0}{EA} = \frac{F_L a_0}{EA}\alpha, \qquad e_C = \frac{F_C a_0}{EA} \tag{3}$$

The compressive forces (F_L and F_C) in the lateral and central members relate to each other through the angle of inclination θ as $F_L\cos\theta = F_C$. The current length of the central member is $e_C = a - a_0$ and that of lateral members is $e_L = L - L_0$. The current truss height h and member length L define the angle of the inclination of the lateral members

$$\cos\theta = \frac{L_x}{L} = \frac{L_x}{\sqrt{L_x^2+h^2}} \tag{4}$$

For the lateral members, the horizontal extension is denoted as L_x, which can be defined as $L_x = (L_T - a)/2 = (L_T - a_0 - e_C)/2$. The elongation of the lateral members can be expressed from the current and initial member length

$$e_L = \sqrt{L_x^2+h^2} - L_0 \tag{5}$$

The compatibility condition is

$$e_C\alpha\ \sec\theta = e_L \text{ or } \frac{\alpha\sqrt{L_x^2+h^2}}{L_x}(L_T - a_0 - 2L_x) = \sqrt{L_x^2+h^2} - L_0 \tag{6}$$

From Eq. (6), solutions for L_x are obtained numerically in dependence of h (thus v) by solving a fourth-order equation. The vertical reaction force in the central Mises truss $R_{y,1}$ is then

$$\begin{aligned} R_{y,1} &= 2hEA\left(\frac{1}{\sqrt{L_x^2+h^2}} - \frac{1}{L_0}\right) \\ &= 2(H_0 - v)EA\left(\frac{1}{\sqrt{L_x^2+H_0^2-2H_0v+v^2}} - \frac{1}{L_0}\right) \end{aligned} \tag{7}$$

The assembly structure imposes the displacement loading condition v_i for each of the Mises trusses corresponding to each force network path (F1, F2, and F3 in Fig. 2(b)). For each force network path (truss i), the ratio $d_i = v_i/v$ is defined, which relates the local displacement to the applied displacement. For the present configuration in particular, one central Mises truss ($i = 1$) and $(N-3)/2$ additional Mises trusses exist.

$$d_1 = 1, \quad d_{1+i} = \frac{\left(\frac{N+1}{2}\right) - i}{\left(\frac{N+1}{2}\right)}, \quad i = \left[1, \frac{(N-3)}{2}\right] \tag{8}$$

The mechanical response of the entire assembly, Eq. (7), is computed from R_{yi} versus v_i for each of the equivalent internal Mises trusses. The overall response of the TIM system is then obtained by summation of individual contributions:

$$R_y = R_{y,1}(v) + 2\cdot\sum_{i=1}^{(N-3)/2} R_{y,i+1}(vd_{i+1}) \tag{9}$$

For the central Mises truss, the tangent stiffness $K(v)$ and the initial stiffness $K(v=0)$ are

$$\begin{aligned} &\frac{\partial R_{y,1}}{\partial v} = K_1(v) \\ &= 2EA\left[\frac{H_0(H_0 - v - L_xL_x')}{(H_0^2 - 2H_0v + L_x^2 + v^2)^{3/2}} + \frac{1}{L_0} - \frac{H_0^2 - H_0v - vL_xL_x' + L_x^2}{(H_0^2 - 2H_0v + L_x^2 + v^2)^{3/2}}\right] \end{aligned} \tag{10}$$

$$\begin{aligned} K_1(v=0) &= 2\left[\frac{EA}{L_0} - \frac{EA(H_0L_{x0}L_{x0}' + L_{x0}^2)}{(H_0^2 + L_{x0}^2)^{3/2}}\right] \\ &= 2EA\left(\frac{L_0^2 - H_0L_{x0}L_{x0}' - L_{x0}^2}{L_0^3}\right) \end{aligned} \tag{11}$$

where $L_x' = dL_x/dv$ and $L_{x0}' = (dL_x/dv)(v=0)$. For the assembly overall, the initial stiffness is obtained from the contribution of all Mises trusses:

$$\begin{aligned} K^* &= \left(1 + 2\cdot\sum_{i=1}^{(N-3)/2} d_{i+1}\right)K_1(v=0) \\ &= \left[1 + 2\cdot\sum_{i=1}^{(N-3)/2}\frac{\left(\frac{N+1}{2}\right) - i}{\left(\frac{N+1}{2}\right)}\right]EA\left\{\frac{1 - \frac{(N-1)^2}{8+(N-1)^2}}{a_0\sqrt{\frac{1}{2}+\frac{(N-1)^2}{16}}} - \frac{\frac{32(N-1)^2}{a_0[8+(N-1)^2]^{5/2}}}{\frac{(N-1)^2}{8+(N-1)^2} + \sqrt{2+\frac{(N-1)^2}{4}}}\right\} \end{aligned} \tag{12}$$

Considering further simplifications and considering $A = \lambda a_0^2$, where λ characterizes the cross-sectional area of the force network path,

$$K = \left(\frac{N^2+2N-7}{N+1}\right)E\lambda a_0\left\{\frac{32}{[8+(N-1)^2]^{3/2}} - \frac{32(N-1)^2}{[(N-1)^2(8+(N-1)^2)^{3/2}+(1/2)(8+(N-1)^2)^3]}\right\} \tag{13}$$

An approximation for the TIM system stiffness (K^*) is obtained from Eq. (13) for values $N > 7$:

$$K^* = 32E\lambda a_0 N^{-2} \tag{14}$$

As the assembly must follow the response of a Mises truss, the deflection to reach the maximum force is proportional to H. The load carrying capacity of the TIM system is then estimated as F^*

$$F^* = K^*(\eta a_0) = 32E\eta\lambda a_0^2 N^{-2} \tag{15}$$

where ηa_0 is the deflection at which the linearized TIM system (described with K^*) reaches the value of the load carrying capacity of the actual TIM system. The value of η is dependent on the sequence of loading the internal Mises trusses. Finally, the geometry of the assembly allows for the calculation of the deflection to reach failure. The condition that the outermost truss, i.e., number $(N-3)/2$, locally reaches a deflection of $v = H_0$, establishes the applied v at final failure as

$$v_f = a_0(N+1)/(4\sqrt{2}) \tag{16}$$

The area under the force-deflection curve W^*, approximated as a triangle, is the toughness of the material system:

$$W^* = \frac{1}{2}F^* v_f = 2\sqrt{2}E\eta\lambda a_0^3 N^{-2}(N+1) \approx 2\sqrt{2}E\eta\lambda a_0^3 N^{-1} \tag{17}$$

4 Results

4.1 Model Analysis and Model Validation. The model is implemented in MATLAB, and numerical solutions for the fourth-order equation are obtained. For the following, the cases of $N = 7$ and $N = 11$ are considered. The case $N = 7$ corresponds to Fig. 2, and there exists a central Mises truss (F1) and two additional pairs of Mises trusses (F2 and F3) such that $d_1 = 1$(F1), $d_2 = 3/4$ (F2), $d_3 = 1/2$ (F3). In the case of $N = 11$, there is a central Mises truss and four pairs of additional trusses with $d_1 = 1$ (F1), $d_2 = 5/6$ (F2), $d_3 = 2/3$ (F3), $d_4 = 1/2$ (F4), $d_5 = 1/3$ (F5). Figure 4 depicts the overall force-deflection response ($R_y - v$) together with the individual contribution of the central truss and the additional trusses (pairs) $R_{yi} - v_i$. The model describes a force-deflection response that is initially linear. A peak force is reached as the load carrying capacity of the equivalent Mises trusses starts to decline. The ratio $F^*/(K^* a_0) = \eta$ is determined as approximately 0.2 and can subsequently be used in Eqs. (15) and (17). Subsequently to reaching the load carrying capacity, the force declines gradually as individual Mises trusses lose their capacity to carry load. The final failure is reached once the outer most Mises truss loses the capacity to carry load. This overall force-deflection response is in excellent qualitative agreement with the experimental data [2,4,7,9,12].

To validate the model, a comparison with a direct numerical simulation model by the use of finite element simulations of TIM assemblies is conducted. Details of the FE model are based on Ref. [15]. The FE computations considered $a_0 = 25$ mm, $E =$ 1.827 GPa, and $\nu = 0.33$. The contact model is a "hard" contact relationship that minimizes the penetration of the slave surface into the master surface (ABAQUS). The coefficient of friction was set to a high numerical value ($\mu = 100$) to minimize the slip between building blocks, with details on the influence of friction on the TIM system response given in Ref. [10]. The validation test is considered successful if for one TIM system configuration (here $N = 7$), the analytical model can be calibrated to the FE model using solely the maximum load computed with the FE model. Then, the analytical model is validated if (1) the remainder of the force-deflection response for $N = 7$ matches that of the FE model computation and (2) the analytical model calibrated at $N = 7$ is also successful in predicting the response computed with the FE model for $N = 11$ without any further model adjustment. In the calibration process, the value of the parameter λ (Eq. (14)) is determined as 0.8.

Figure 5(a) depicts the results for the force-deflection response for the case $N = 7$. The analytical model is calibrated to the maximum force, and with this calibration, the analytical model predicts the overall force-deflection record in excellent agreement with

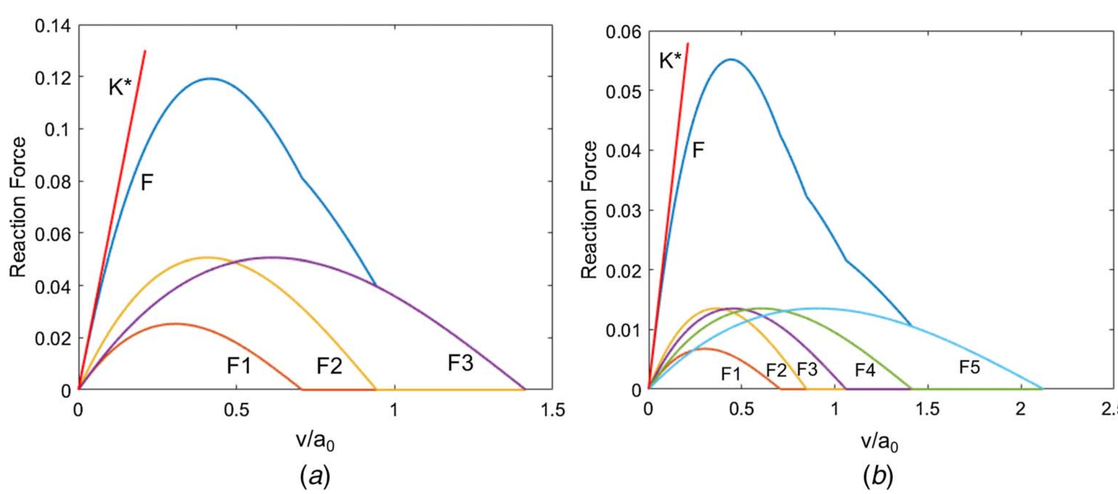

Fig. 4 The force-deflection response of the TIM system emerges from the summation of the response of individual Mises trusses representing the load transfer in selected rows of the tetrahedra assembly: (*a*) for $N = 7$, the overall force F (and stiffness K*) emerges from Mises trusses F1, F2, and F3 and (*b*) for $N = 11$ the overall force F (and stiffness K*) emerges from Mises trusses F1, F2, F3, F4, and F5 ($E\lambda a_0 = 1$ [N])

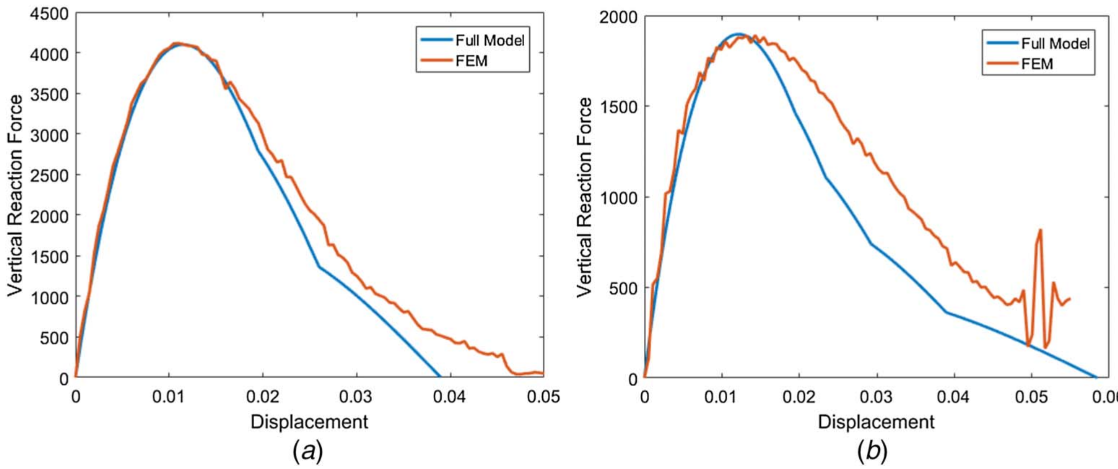

Fig. 5 Comparison between force-deflection response from the analytical model and direct numerical simulation: (*a*) $N=7$ is used for model calibration and (*b*) $N=11$ is prediction without further parameter fit

the FE model. Figure 5(*b*) depicts the results for the case of $N=11$. The analytical model, calibrated with the FE model maximum force at $N=7$, is able to predict the entire force-deflection response obtained with the FE model without further calibration.

4.2 Behavior of Topologically Interlocked Material Systems of Varying Assembly. The model for the computation of the transverse loading response is now used to compute the transverse stiffness K^* [10], maximum load carrying capacity F^*, and toughness W^* (for three sets of TIM system configurations, Fig. 6).

For the size case (Fig. 6(*a*)), the results of the analysis are given in Fig. 7. An increase in the size of the building block a_0 and keeping the number of building blocks the same ($N=\text{const.}0$) increases the transverse stiffness of the assembly [10] and increases the load carrying capacity. Both the normalized deflection (v/a_0*

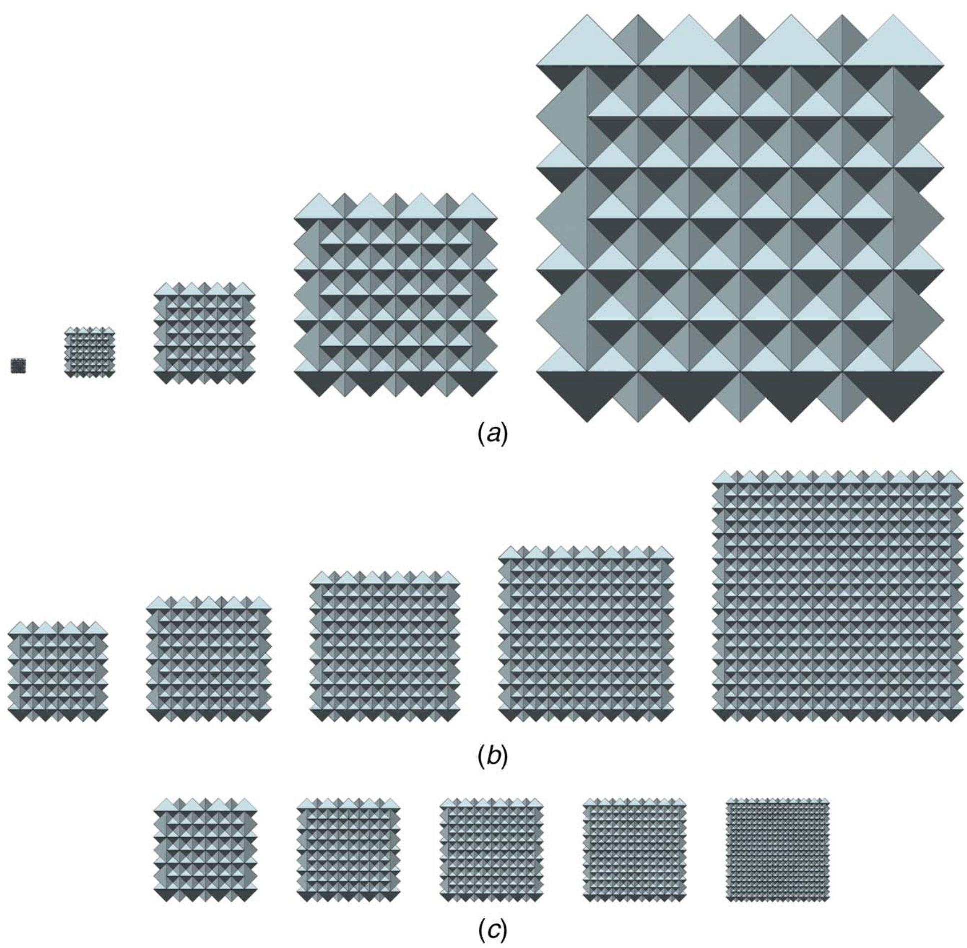

Fig. 6 Assemblies considering (*a*) a change in the size of the unit element (size), (*b*) a change in the number of unit elements of a given size (growth), and (c) a change in the number of unit elements in a given assembly domain (scaling)

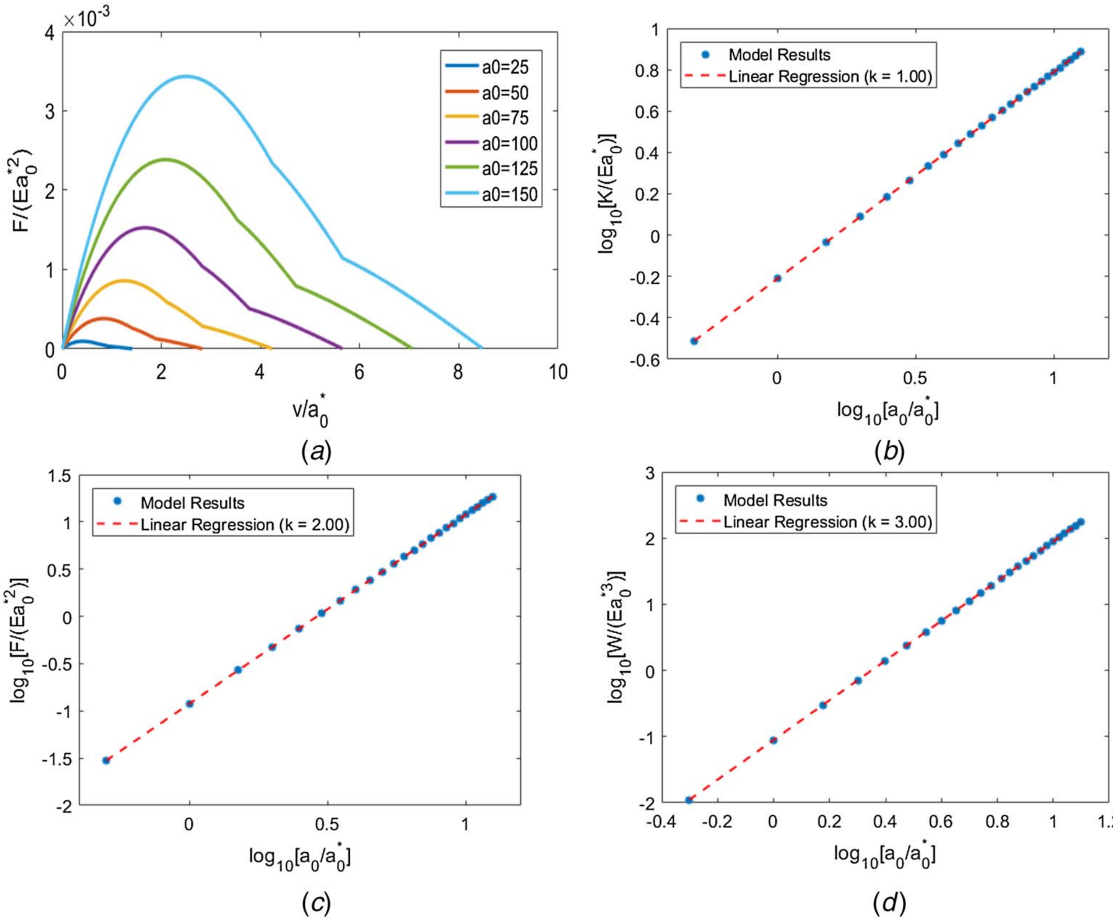

Fig. 7 Size of the TIM system (N = const., a_0 varying): (*a*) force-deflection response, (*b*) stiffness versus building block dimensions, (*c*) load carry capacity versus building block dimensions, and (*d*) toughness versus building block dimensions

with a_0* a references unit size) to reach peak load also and the normalized deflection at which final loss of load occurs increase with a_0. Following Eqs. (14), (15) and (17), stiffness scales as (a_0/a_0*), strength as $(a_0/a_0*)^2$, and toughness as $(a_0/a_0*)^3$. These exponents are in good agreement with the results of the analysis of the full model (Figs. 7(*b*)–7(*d*)). The relationship between toughness and load carrying capacity is $W^* \propto (F^*)^{3/2}$.

For the growth case (Fig. 6(*b*)), the results of the analysis are given in Fig. 8. An increase in the number N of identical building block with size a_0 decreases the transverse stiffness of the assembly [10] as well as the load carrying capacity. The normalized deflection (v/a_0) to reach the peak load remains constant but the normalized deflection at which the final loss of load occurs increases with N. Following Eqs. (14), (15) and (17), stiffness scales as N^{-2}, strength as N^{-2}, and toughness as N^{-1}. These exponents are in good agreement with the results of the analysis of the full model for stiffness and load carrying capacity (Figs. 8(*b*) and 8(*c*)). The predictions of the full model (Fig. 8(*c*)) and Eq. (17) deviate in their prediction of the toughness W^*, an outcome attributed to the change of in shape of the force-deflection curve with changing N (Fig. 8(*a*)). The relationship between toughness and load carrying capacity is $W^* \propto (F^*)^{1/2}$ following Eqs. (15) and (17) and $W^* \propto (F^*)^{0.79}$ from the full model.

For the scaling case (Fig. 6(*c*)), the results of the analysis are given in Fig. 9. Here, the constraint of constant in-plane dimension of the TIM system is considered as $Na_0 = \text{const}$. An increase in the number N of building blocks with size proportional to $a_0 \propto N^{-1}$ decreases the transverse stiffness of the assembly [10] as well as the load carrying capacity. The normalized deflection (v/a_0) to reach the peak load also declines but the normalized deflection at which final loss of load occurs remains constant. Following Eqs. (14), (15), and (17), stiffness scales as N^{-3}, strength as N^{-4}, and toughness as N^{-4}. These exponents are in good agreement with the results of the analysis of the full model for stiffness and load carrying capacity (Figs. 9(*b*) and 9(*c*)). The predictions of the full model (Fig. 9(*c*)) and Eq. (17) deviate in their prediction of the toughness W^*, an outcome attributed again to the change of in shape of the force-deflection curve with changing N (Fig. 9(*a*)). The relationship between toughness and load carrying capacity is $W^* \propto (F^*)$ following Eqs. (15) and (17) and $W^* \propto (F^*)^{1.15}$ from the full model.

5 Discussion

It is useful to compare the behavior of the TIM assemblies to conventional monolithic plates. For comparison, a plate under simply supported conditions and a central load is considered. This configuration best approximates the boundary conditions imposed on the TIM assembly of the present study. It is assumed that the plate (thickness $t \propto a_0$, in-plane dimension $b \propto L_T$, and load domain diameter $e \propto a_0$) is made of a material with elastic modulus E and that its brittle failure strength σ_f relates to its elastic modulus as $\sigma_f = E/\chi$. Plate stiffness, maximum load, and toughness (again as area under the force-deflection curve) are as follows [16]:

$$K^{\text{plate}} = \frac{E}{k_1}\frac{t^3}{b^2} \propto E\frac{a_0^3}{L_T^2} \sim Ea_0^2N^{-2} \tag{18}$$

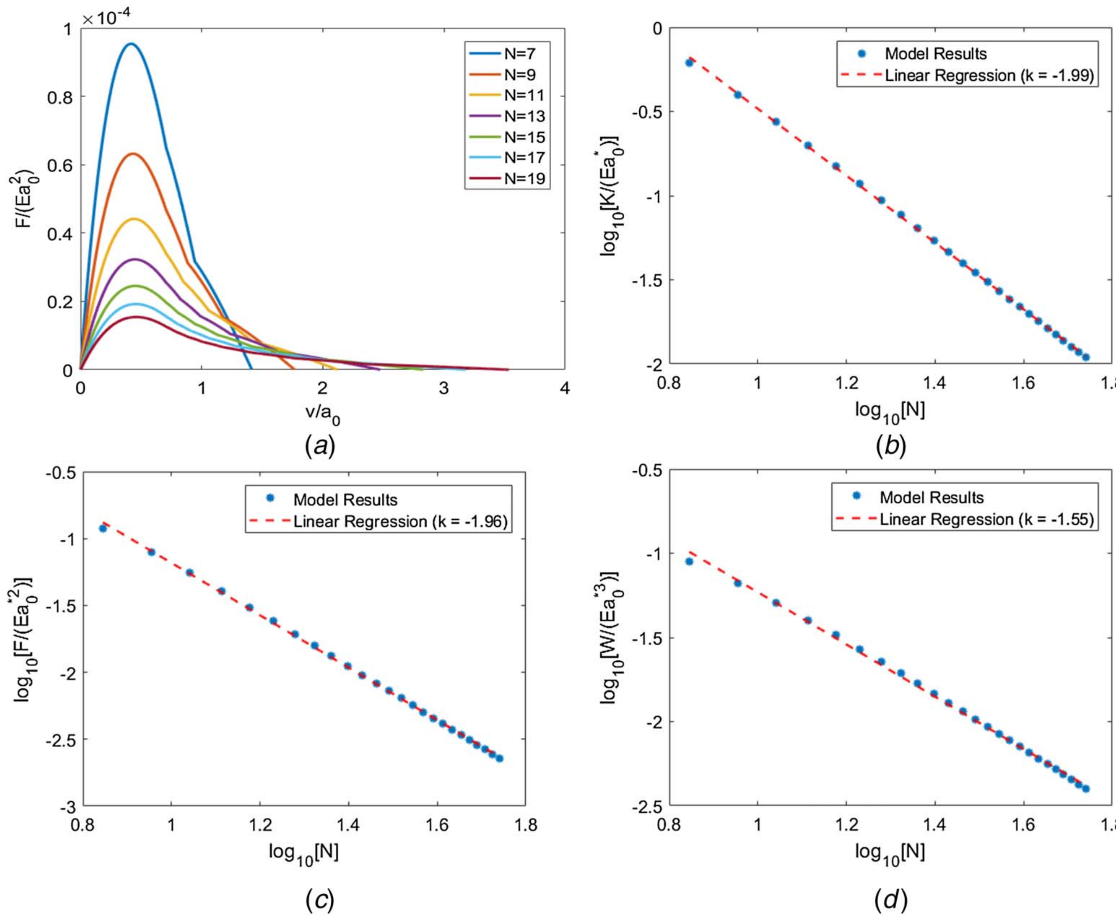

Fig. 8 Growth of the TIM system (a_0 = const., *N* varying): (*a*) force-deflection response, (*b*) stiffness versus building block dimensions, (c) load carry capacity versus building block dimensions, and (*d*) toughness versus building block dimensions

$$F_{\max}^{\text{plate}} = \frac{\sigma_f t^2 \pi}{1.5\left[(1+\nu)\ln\left(\dfrac{2b}{\pi e}\right) + k_2\right]} \propto \frac{(E/\chi)a_0^2}{\ln(N)} \tag{19}$$

$$W^{\text{plate}} = \frac{1}{2}\frac{\left(P_{\max}^{\text{plate}}\right)^2}{K^{\text{plate}}} = \frac{1}{2}\frac{\sigma_f^2}{E}\frac{tb^2}{\ln(b/\pi e)} \propto \frac{1}{2}\frac{E}{\chi^2}a_0^2 N^{3/2} \tag{20}$$

Comparing Eqs. (14)–(19), it is seen that the TIM assembly approach provides a different scaling of properties than the monolithic plate, except for stiffness for which the plate and the TIM assembly are found to scale the same way with thickness and in-plane dimension. This finding is relevant if it is desired to alter relative relationships between stiffness, strength, and toughness. A critical value of χ is determined as

$$\hat{\chi} \sim N^{3/2} \tag{21}$$

for which the TIM system with element size a_0 would provide higher maximum force than the corresponding plate. Similarly, a critical value of χ is determined as

$$\tilde{\chi} \sim a_0^{1/2} N^{1/4} \tag{22}$$

for which the TIM system would provide higher toughness than the corresponding monolithic plate. While these comparisons are somewhat limited by the range of good validity of the plate theories for all combinations of Na_0, the analysis nevertheless indicates that TIM systems are a potential viable solution for structures to be built from low strengths materials. For such TIM systems, both strength and toughness are larger than those for the monolithic plate. The comparison of $\hat{\chi}$ to $\tilde{\chi}$ indicates that TIM systems are more suited to the case where toughness is the desired property as it is much easier to realize a TIM systems that exceed the monolithic plate in toughness than in load carrying capacity. This outcome of the analysis is in good qualitative agreement with experimental results in Ref. [12]. These authors demonstrate that for a TIM system possessing similar load carrying capacity as the corresponding monolithic plate, the toughness of the TIM system far exceeds that of the monolithic plate.

Further investigations on the effects of boundary conditions (simply supported versus clamped) and the loading conditions could be considered as further steps even for the TIM system based on tetrahedra. The present model is limited to conditions where slip does not play a role. The incorporation of additional components of sliding would allow for a realistic representation of experimental conditions. As architecture plays a central role in the TIM systems and determined the force network structure, it is also necessary to establish variants of the present theory for TIM systems with building blocks other than the tetrahedra.

6 Conclusion

This paper provides a model for the analysis of the deflection under transverse loading of a 2D architectured material system constructed as a topologically interlocked assembly of tetrahedra. Photoelastic experiments were used to aid in providing insight into the internal force network. The force network structure is translated into a model where trusses are used to represent the TIM

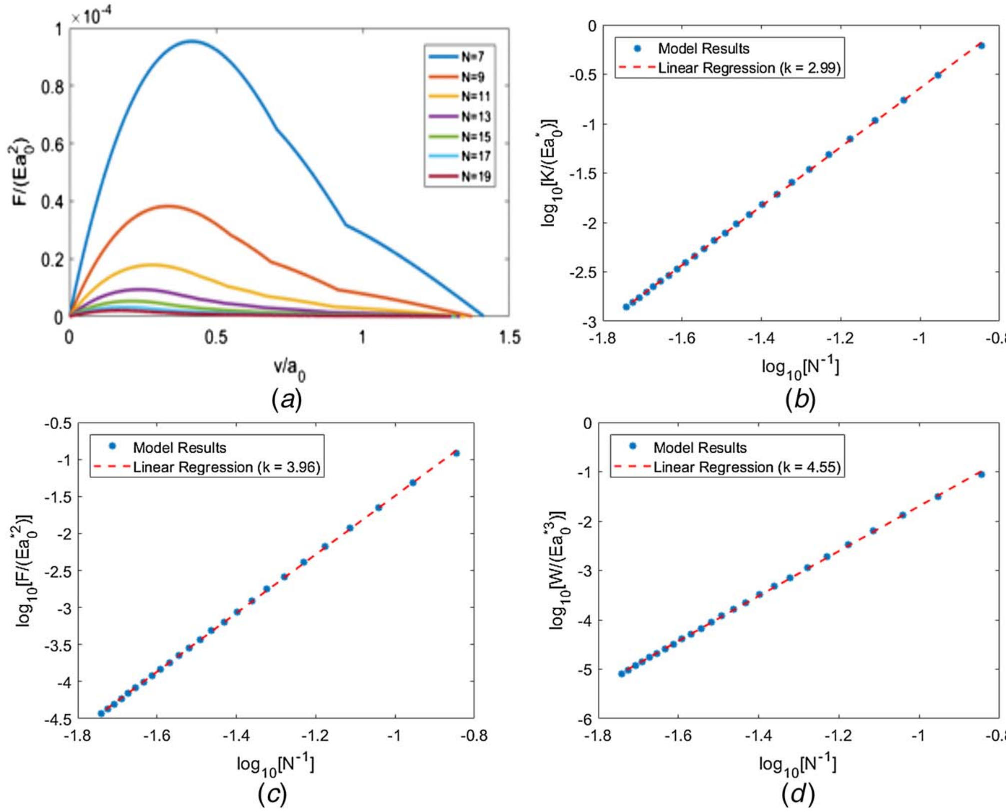

Fig. 9 Scaling of the TIM system ($Na_0 = \text{const.}$): (*a*) force-deflection response, (*b*) stiffness versus building block dimensions, (*c*) load carry capacity versus building block dimensions, and (*d*) toughness versus building block dimensions

system. The theory leads to a solution for the full force-deflection record for the TIM system under simple support and transverse point loading. In addition, closed-form equations for stiffness, load carrying capacity, and toughness of a model TIM system has been presented. Model predictions are in good quantitative agreement with direct numerical simulations and in good qualitative agreement with findings in the related experiment. It is demonstrated that the TIM system possesses scaling relationships that differ from those of equivalent monolithic systems. Thus, TIM systems provide new approaches to mechanically loaded 2D structures with the TIM systems of particular relevance if brittle materials with high modulus to stiffness ratio are of concern.

Acknowledgment

Qichang Chu's contribution to the photoelastic experiments is gratefully acknowledged. He was supported by a Bottomley Scholarship for undergraduate research in the School of Mechanical Engineering at Purdue University.

Funding Data

- National Science Foundation under Grant No. 1662177 (Funder ID: 10.13039/501100008982).

References

[1] Reddy, J. N., 2006, *Theory and Analysis of Elastic Plates and Shells*, CRC Press, Boca Raton, FL.

[2] Dyskin, A. V., Estrin, Y., Kanel-Belov, A. J., and Pasternak, E., 2001, "Toughening by Fragmentation—How Topology Helps," Adv. Eng. Mat., **3**(11), pp. 885–888.

[3] Ashby, M. F., and Bréchet, Y. J. M., 2003, "Designing Hybrid Materials," Acta Mater., **51**(19), pp. 5801–5821.

[4] Dyskin, A. V., Estrin, Y., Kanel-Belov, A. J., and Pasternak, E., 2003, "A New Principle in Design of Composite Materials: Reinforcement by Interlocked Elements," Compos. Sci. Technol., **63**(3–4), pp. 483–491.

[5] Siegmund, T., Barthelat, F., Cipra, R., Habtour, E., and Riddick, J., 2016, "Manufacture and Mechanics of Topologically Interlocked Material Assemblies," ASME Appl. Mech. Rev., **68**(4), p. 040803.

[6] Dugue, M., Fivel, M., Brechet, Y., and Dendievel, R., 2013, "Indentation of Interlocked Assemblies: 3D Discrete Simulations and Experiments," Comp. Mat. Sci., **79**, pp. 591–598.

[7] Khandelwal, S., Siegmund, T., Cipra, R. J., and Bolton, J. S., 2012, "Transverse Loading of Cellular Topologically Interlocked Materials," Int. J. Solids Struct., **49**(18), pp. 2394–2403.

[8] Dyskin, A. V., Pasternak, E., and Estrin, Y., 2012, "Mortarless Structures Based on Topological Interlocking," Front. Struct. Civ. Eng., **6**(2), pp. 188–197.

[9] Mather, A., Cipra, R., and Siegmund, T., 2012, "Structural Integrity During Remanufacture of a Topologically Interlocked Material," Int. J. Struct. Integ., **3**(1), pp. 61–78.

[10] Khandelwal, S., Siegmund, T., Cipra, R. J., and Bolton, J. S., 2014, "Scaling of the Elastic Behavior of Two-Dimensional Topologically Interlocked Materials Under Transverse Loading," ASME J. Appl. Mech., **81**(3), p. 031011.

[11] Brocato, M., 2018, "Continuum Mechanics—A Continuum Model of Interlocking Structural Systems," Rend. Lincei Mat. Appl., **29**(2018), pp. 63–83.

[12] Mirkhalaf, M., Zhou, T., and Barthelat, F., 2018, "Simultaneous Improvements of Strength and Toughness in Topologically Interlocked Ceramics," PNAS, **37**(115), pp. 9128–9133.

[13] Conway, J. H., and Torquato, S., 2006, "Packing, Tiling, and Covering With Tetrahedra," PNAS, **103**(28), pp. 10612–10617.

[14] Daniels, K. E., Kollmer, J. E., and Puckett, J. G., 2017, "Photoelastic Force Measurements in Granular Materials," Rev. Sci. Instr., **88**(5), p. 051808.

[15] Feng, Y., Siegmund, T., Habtour, E., and Riddick, J., 2015, "Impact Mechanics of Topologically Interlocked Material Assemblies," Int. J. Impact Eng., **75**(1), pp. 140–149.

[16] Young, W. C., Budynas, R. G., and Sadegh, A. M., 2002, *Roark's Formulas for Stress and Strain*, Vol. 7, McGraw-Hill, New York.